

---

# Time Series Continuous Modeling for Imputation and Forecasting with Implicit Neural Representations

---

Etienne Le Naour\*<sup>1,2</sup>, Louis Serrano\*<sup>1</sup>, Léon Migus\*<sup>1,3</sup>, Yuan Yin<sup>1</sup>, Ghislain Agoua<sup>2</sup>  
 Nicolas Baskiotis<sup>1</sup>, Patrick Gallinari<sup>1,4</sup>, Vincent Guigue<sup>5</sup>

<sup>1</sup> Sorbonne Université, CNRS, ISIR, 75005 Paris, France

<sup>2</sup> EDF R&D, Palaiseau, France

<sup>3</sup> Sorbonne Université, CNRS, Laboratoire Jacques-Louis Lions, 75005 Paris, France

<sup>4</sup> Criteo AI Lab, Paris, France

<sup>5</sup> AgroParisTech, Palaiseau, France

{*louis.serrano, leon.migus, yuan.yin, nicolas.baskiotis, vincent.guigue*}@sorbonne-universite.fr

{*etienne.le-naour, ghislain.agoua*}@edf.fr

## Abstract

Although widely explored, time series modeling continues to encounter significant challenges when confronted with real-world data. We propose a novel modeling approach leveraging Implicit Neural Representations (INR). This approach enables us to effectively capture the continuous aspect of time series and provides a natural solution to recurring modeling issues such as handling missing data, dealing with irregular sampling, or unaligned observations from multiple sensors. By introducing conditional modulation of INR parameters and leveraging meta-learning techniques, we address the issue of generalization to both unseen samples and time window shifts. Through extensive experimentation, our model demonstrates state-of-the-art performance in forecasting and imputation tasks, while exhibiting flexibility in handling a wide range of challenging scenarios that competing models cannot.

## 1 Introduction

Time series analysis and modeling have become increasingly important in a wide range of fields, including industry, medicine, and climate science. With the increasing number of deployed sensors, a significant amount of time series data has become available, creating new opportunities for Deep Learning (DL) models. Among these time series a wide part are instances of univariate phenomena observed from diverse locations, such as electricity consumption<sup>1</sup> and road traffic<sup>2</sup>. Each individual's time series displays distinctive variations, while still sharing a common underlying phenomenon.

In this paper, we focus on these univariate time series with multiple instances/samples and address two critical tasks: imputation and long-term time series forecasting (LTSF).

In recent years, DL methods have been quite effective in addressing imputation tasks as in Cao et al. (2018); Du et al. (2023), as well as LTSF, as in Zeng et al. (2022); Nie et al. (2022). However, applying these approaches to real-world data presents significant challenges, including the following:

---

\* Equal contribution

<sup>1</sup><https://archive.ics.uci.edu/ml/datasets/ElectricityLoadDiagrams20112014>

<sup>2</sup><https://pems.dot.ca.gov/>

(i) The samples may not always be available at the same time window. Practical considerations, such as the installation of new sensors, or legal restrictions, such as the EU GDPR, may prevent the simultaneous availability of all samples over time. As a result, it becomes critical to have a model that exhibits generalizability to new samples, while most deep learning methods for imputation and forecasting explicitly capture the relationships between samples. (ii) In many scenarios, time series are observed at irregular time steps (Clark and Bjørnstad, 2004; Schulz and Stattegger, 1997), which limits the application of most existing deep learning methods which are inflexibly designed for series on a regular grid. In the context of imputation, it implies that the ground truth series share the same grid. In the context of forecasting, it implies that the look-back window is a dense and regular grid. However, if there are any gaps or missing values within this dense grid, the performance of these models can be significantly degraded, resulting in a negative impact on their forecasting accuracy (Chen et al., 2001; Kim et al., 2019).

The above issues go beyond the assumptions of current models, making most effective deep learning models such as Wu et al. (2021); Zeng et al. (2022); Du et al. (2023) inappropriate or inapplicable to the real-world data. To overcome these challenges, we need a model that generalizes to unseen samples during training, that handles arbitrary sampling grids in time and is robust to missing values. Therefore, a continuous model which allows a unified solution for different tasks seems an appropriate and elegant choice.

Implicit neural representations (INRs) have recently gained attention for their ability to represent high-frequency functions using neural networks. This approach enables continuous modeling of the data, eliminating the need for discretization or interpolation, and providing a more flexible and efficient alternative to traditional approaches. Moreover, recent attempts at continuous modeling with INRs have shown promising results in many domains, such as image generation (Dupont et al., 2022) or dynamics modeling (Yin et al., 2023). Therefore, we believe that applying such a framework to time series modeling is a logical next step.

To address the above limitations, we introduce TimeFlow, an approach that uses INR to model univariate time series as continuous functions of time. To allow the INR to efficiently represent multiple samples, we condition it by a per-sample code, learnable in the latent space. This allows effective generalization to new samples and time windows by modulating the network.

The properties of INRs provide a solution to the challenge posed by irregular time steps, allowing us to tackle both imputation and forecasting tasks for non-stationary time series. In summary, our work makes the following key contributions:

- Our proposed framework is a modulated INR that can effectively model univariate time series with multiple individuals as a continuous function of time. To the best of our knowledge, we are one of the first to adapt INR to tackle imputation and forecasting tasks simultaneously for continuous modeling.
- Our results demonstrate state-of-the-art performance compared to leading deep learning models for imputation. In addition, our approach demonstrates the ability to effectively adapt to new samples and time windows.
- We demonstrate that our model not only performs as well as state-of-the-art deep learning models for long-term forecasting but also has the ability to adapt to new samples. Furthermore, our approach outperforms existing models by offering enhanced flexibility, allowing for accurate forecasting even in the presence of missing values.

## 2 Related work

**Deep Learning for time series imputation** In recent years, Deep Learning (DL) methods have been widely used for time series imputation. One of the first pioneering methods to achieve success is BRITS (Cao et al., 2018) which uses a bidirectional recurrent neural network (RNN). Subsequently, DL methods were later explored, starting with GAN-based approaches (Luo et al., 2018, 2019; Liu et al., 2019), then VAE (Fortuin et al., 2020) and diffusion models (Tashiro et al., 2021). While these approaches perform comparably to BRITS, they often have more challenging training requirements and longer inference times. More recently, transformers have been successfully applied to imputation, as in SAITS (Du et al., 2023). In addition, TIDER (Liu et al., 2023) tackles long time series with a disentangled temporal representation. These methods provide SOTA results while

being less computationally expensive than generative methods. However, none of these methods generalize to new samples without retraining the entire model, nor do they handle irregular time series.

**Deep Learning for time series forecasting** Most recent DL forecasting models are based on transformers. Initial approaches directly use transformers to forecast (Zhou et al., 2021; Liu et al., 2022; Wu et al., 2021; Zhou et al., 2022) using pointwise input tokens. However, the recent work DLinear (Zeng et al., 2022) show that simpler one-layer linear models, which take trend and seasonal context into account, outperformed initial transformers, highlighting the importance of the contextual information. PatchTST (Nie et al., 2022) addresses this issue by considering longer tokens to take the context into account. All these models are autoregressive, and none can handle irregularly sampled look-back windows. Also, only PatchTST can generalize to new samples.

**Time series continuous modeling** Gaussian processes (Rasmussen and Williams, 2006) were initially used to model time series as continuous functions, but they require the selection of an appropriate kernel, which assumes strong prior (Corani et al., 2021). Another commonly used continuous model is Prophet (Taylor and Letham, 2017), which requires incorporating priors such as calendar information. Eliminating the need for important priors, Brouwer et al. (2019) and Rubanova et al. (2019) model time series with continuous latent spaces defined by ordinary differential equations. mTAN (Shukla and Marlin, 2021) uses an attention mechanism to learn a fixed-length representation for irregular multivariate time series, that can be used for interpolation. While these approaches have shown significant progress in continuous modeling for time series, they are less efficient than the aforementioned autoregressive models for regularly observed time series and cannot extrapolate for complex dynamics.

**Implicit neural representation** The recent development of implicit neural representations (INRs) has led to impressive results in computer vision (Sitzmann et al., 2020; Tancik et al., 2020; Fathy et al., 2021; Mildenhall et al., 2021). These networks can represent data as a continuous function, queryable with coordinates. While they have been applied in other fields such as physics (Yin et al., 2023) and meteorology (Huang and Hoefler, 2023), little time series research has been done on INRs. Initial research (Fons et al., 2022; Jeong and Shin, 2022) focused on generation and anomaly detection, while Woo et al. (2022) explored long-term forecasting. However, they are still limited by their fixed grid input requirement, which prevents them from fully benefiting from the continuous aspect of INRs.

### 3 Method

In this section, we present TimeFlow, a modulated-INR architecture that can be used to reconstruct, impute and forecast univariate time series with multiple samples.

**Overview** Our method aims to alleviate the dependence on fixed sampling. We propose to represent the time series  $x_t$  by a time-continuous function  $f(t)$  that can be queried at any time  $t$ . To this end, we use a recent DL approach called implicit neural representation (INR), which can learn from discrete data a neural network  $f_\theta(t)$  that can output the value at any time  $t$ . However, a single INR can represent only one time series. To represent a set of time series, instead of retraining multiple INRs, we propose to modulate the parameters  $\theta$  of the INR in a latent space through a per-sample code. This allows efficient representation of a set of time series with INR and also allows gathering the shared information across the sample. This modification is generated by a hypernetwork, which takes the code as input and outputs the modification. Therefore, the INR and the hypernetwork are two key components of our model. We will discuss them in detail below.

**INR** Formally, an INR is a parameterized continuous function  $f_\theta$  that maps coordinates of dimension  $m$  to their corresponding function values, a vector of dimension  $d$ , i.e.,  $f_\theta: \mathbb{R}^m \rightarrow \mathbb{R}^d$ . For example, a 2D RGB image is a mapping from pixel coordinates of dimension  $m = 2$  to the corresponding pixel values  $d = 3$ . The INR is usually implemented by a MLP with modified inputs and a specific activation function to efficiently represent high frequency details in the data, as empirically demonstrated for images in Sitzmann et al. (2020); Tancik et al. (2020).

In our case, the network models the time series  $x_t$  as a function of a time coordinate  $t$ . Fitting an INR amounts to minimizing a reconstruction loss between an observed series  $x_t$  and its approximation  $\tilde{x}_t = f_\theta(t)$ . The time continuity property is guaranteed by the network’s ability to be queried at any point in time.

**Hypernetwork** To reconstruct different univariate time series  $(x_t^{(j)})_{j=1}^n$  with an INR  $f_\theta$ , we modulate the weights  $\theta$  of the coordinate-based network with a hypernetwork  $h_w$ . For a time series  $x_t^{(j)}$ , the hypernetwork maps a latent code  $z^{(j)} \in \mathbb{R}^{d_z}$  containing specific knowledge about the time series to  $\mathbb{R}^{|\theta|}$  the parameter space of the INR.

In practice, we implement an efficient hypernetwork by choosing a linear hypernetwork and applying only shift modulations, i.e., mapping linearly the code to modulations that only modify the biases of the network. More precisely, the output of the  $l$ -th layer of the MLP is given by  $\phi_l = \sigma(\theta_l \phi_{l-1} + b_l + W_l z^{(j)})$ . We denote the modulated INR as  $f_{\theta, h_w(z^{(j)})}$ , where its outputs are approximations of the time series  $x_t^{(j)}$ . This simplifies the optimization and reduces the total number of parameters.

**Training** To effectively solve the joint learning of the codes and the shared parameters in the INR and the hypernetwork, we adopt a meta-training procedure so that our model learns to adapt the code  $z^{(j)}$  in a few gradient steps for a new series  $x_t^{(j)}$ , while learning the shared parameters. We use the meta-learning approach presented in Dupont et al. (2022), which is based on Zintgraf et al. (2019). At each training epoch and for each batch of data, we first update individually the codes  $z^{(j)}$  in the inner loop, then we update the common parameters in the outer loop. In the inner loop, given a time series  $x_t^{(j)}$ , we optimize the code  $z^{(j)}$  using gradient descent, by minimizing the reconstruction error with the series. The inner loop writes as follows:

$$z_{(0)}^{(j)} = 0; \quad z_{(k)}^{(j)} = z_{(k-1)}^{(j)} - \alpha \nabla_{z_{(k-1)}^{(j)}} \mathcal{L}_{\mu_j}(f_{\theta, h_w(z_{(k-1)}^{(j)})}, x_t^{(j)}) \quad \text{for } 1 \leq k \leq K \quad (1)$$

where  $\alpha$  is the inner-loop learning rate,  $K$  the number of inner steps, and  $\mathcal{L}_{\mu_j}(v_t, w_t) := \mathbb{E}_{t \sim \mu_j}[(v_t - w_t)^2]$ . Note that in our case, the measures  $\mu_j$  can be different from one time series to another, if for instance they do not have the same timestamps.

In practice, doing a small number of steps in the inner loop is enough to train the model to achieve high reconstruction results. This is made possible because we do not detach the gradients at the end of the inner loop during training, which helps the network understand how these codes were obtained in the first place. In contrast with first-order methods, we found that this optimization was more stable and could better fit our data.

**Specificity for Imputation and Forecasting** In the imputation setting, we denote as  $\mathcal{T}_{in}$  the observed grid and  $\mathcal{T}$  the ground truth dense grid ( $\mathcal{T}_{in} \subset \mathcal{T}$ ). In the forecasting setting,  $\mathcal{T}_{in}$  represents the look-back window grid and  $\mathcal{T}_{out}$  the horizon grid. They are both included in the ground truth dense grid  $\mathcal{T}$ . In both cases, we wish to infer the time series in  $\mathcal{T}$  based on the observation of values lying in  $\mathcal{T}_{in}$ . To this extent, we condition the network with the output code  $z_{(K)}$  of the Equation (1) using only the data from  $\mathcal{T}_{in}$ , and learn the shared INR and hypernetwork parameters using  $\mathcal{T}_{in}$ , and  $\mathcal{T}_{out}$  if it exists. When  $\mathcal{T}_{out}$  exists we set  $\lambda = 1$  otherwise  $\lambda = 0$ . The unified training procedure for imputation and forecasting is described in Algorithm 1. The exact training and inference procedure for each setting are detailed in Sections 4.1 and 4.2.

## 4 Experiments

**Datasets** For comparison purposes, we use three extensive univariate datasets that are commonly used in the deep learning literature for imputation and long-term time series forecasting. The *Electricity* dataset includes the hourly electricity load curve of 321 customers in Portugal from 2012 to 2014. The *Traffic* dataset presents road occupancy rates of 862 locations and consists of hourly data collected from freeway sensors in San Francisco between 2015 and 2016. The *Solar* dataset contains solar power production measurements from 137 photovoltaic plants in Alabama. The data was collected in 2006 at 10-minute intervals. We also produce an hourly version (*SolarH*) which is used in the forecasting section to compare the same horizons for each dataset. The time series included

---

**Algorithm 1: TimeFlow Training**


---

**while** no convergence **do**

Sample batch  $\mathcal{B}$  of data  $(x_t^{(j)})_{j \in \mathcal{B}}$ ;  
 Set codes to zero  $z^{(j)} \leftarrow 0, \forall j \in \mathcal{B}$ ;  
**for**  $j \in \mathcal{B}$  and step  $\in \{1, \dots, K\}$  **do**  
    $z^{(j)} \leftarrow z^{(j)} - \alpha \nabla_{z^{(j)}} \mathcal{L}_{\mathcal{T}_{in}^{(j)}}(f_{\theta, h_w}(z^{(j)}), x_t^{(j)})$ ;                      // input encoding inner step  
**end**  
 $\theta \leftarrow \theta - \nabla_{\theta} \frac{1}{|\mathcal{B}|} \sum_{j \in \mathcal{B}} [\mathcal{L}_{\mathcal{T}_{in}^{(j)}}(f_{\theta, h_w}(z^{(j)}), x_t^{(j)}) + \lambda \mathcal{L}_{\mathcal{T}_{out}^{(j)}}(f_{\theta, h_w}(z^{(j)}), x_t^{(j)})]$ ;  
 $w \leftarrow w - \nabla_w \frac{1}{|\mathcal{B}|} \sum_{j \in \mathcal{B}} [\mathcal{L}_{\mathcal{T}_{in}^{(j)}}(f_{\theta, h_w}(z^{(j)}), x_t^{(j)}) + \lambda \mathcal{L}_{\mathcal{T}_{out}^{(j)}}(f_{\theta, h_w}(z^{(j)}), x_t^{(j)})]$ ;  
**end**

---

in the experiments exhibit diversity in several aspects. The *Traffic* and *Electricity* datasets have a variety of frequencies, including daily and weekly seasonality, while the *Solar* dataset has unique daily frequencies. In addition, the *Electricity* dataset displays significant individual variation across samples and stronger trends compared to the *Traffic* and *Solar* datasets. The underlying pattern in the data may be caused by human activity, physical phenomena, or a combination of both.

**Implementation details** In all the following experiments, we use a Fourier features network INR (Tancik et al., 2020) with 5 hidden layers, each of dimension 256. The number of input frequencies is 64, while the latent code dimension is 128. Additional information on the choice of hyperparameters and their influence on the performance can be found in the supplementary material.

#### 4.1 Imputation

First, we address the imputation task, which is a common problem in time series. We address the classical imputation setting, where the series to be imputed are a system consisting of  $n$  univariate samples that are partially observed over a given time window. Using our approach, we can predict the continuum of each individual based on partial observations.

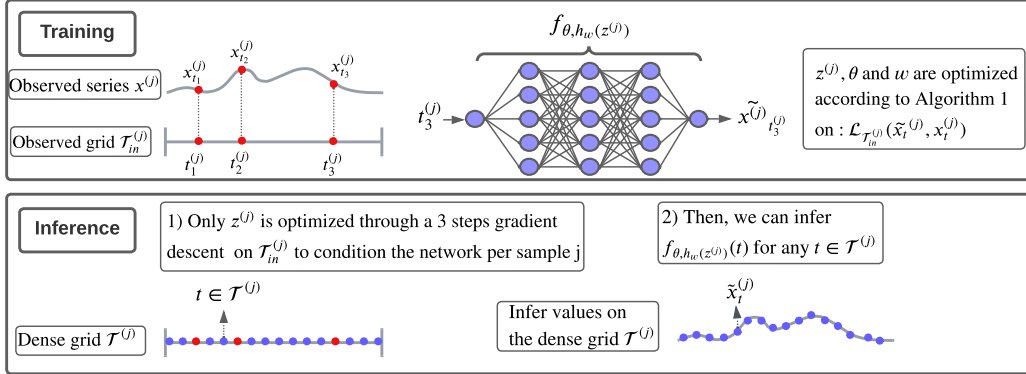


Figure 1: Training and inference procedures for imputation on a fixed grid for known samples

**Setting** For a time series  $x^{(j)}$ , we denote the set of observed points as  $\mathcal{T}_{in}^{(j)}$  and the ground truth set of points as  $\mathcal{T}^{(j)}$ . The observed time grids may be irregularly spaced and may differ across samples. Once the model has been trained using Algorithm 1, the INR for each sample  $j$  is conditioned by  $z^{(j)}$ , which is found by optimizing through the inner loop steps. The entire procedure is illustrated in Figure 1. For comparison with the SOTA imputation baselines, we assume that the ground truth time grid is the same for each individual and that the subsampling rate is the same for each observed time series (i.e.  $\forall (i, j) \in \{1, \dots, n\}^2, |\mathcal{T}_{in}^{(j)}| = |\mathcal{T}_{in}^{(i)}|$  and  $\mathcal{T}^{(j)} = \mathcal{T}^{(i)}$ ). The subsampling rate  $\tau$  of observed values can be defined as  $|\mathcal{T}_{in}^{(j)}|/|\mathcal{T}^{(j)}|$ .

Table 1: Mean MAE imputation results on the missing grid only over five different time window.  $\tau$  stands for the subsampling rate. Bold results are best, underline results are second best.

	$\tau$	TimeFlow	SAITS	BRITS	TIDER	mTAN	Linear	KNN (k=3)
Electricity	0.05	<b>0.324 ± 0.013</b>	0.384 ± 0.019	<u>0.329 ± 0.015</u>	0.427 ± 0.010	0.575 ± 0.039	0.828 ± 0.045	0.531 ± 0.033
	0.10	<b>0.250 ± 0.010</b>	0.308 ± 0.011	<u>0.287 ± 0.015</u>	0.399 ± 0.009	0.412 ± 0.047	0.716 ± 0.039	0.416 ± 0.020
	0.20	<b>0.225 ± 0.008</b>	0.261 ± 0.008	<u>0.245 ± 0.011</u>	0.391 ± 0.010	0.342 ± 0.014	0.518 ± 0.029	0.363 ± 0.019
	0.30	<b>0.212 ± 0.007</b>	0.236 ± 0.008	<u>0.221 ± 0.008</u>	0.384 ± 0.009	0.335 ± 0.015	0.396 ± 0.022	0.342 ± 0.017
	0.50	<u>0.194 ± 0.007</u>	0.209 ± 0.008	<b>0.193 ± 0.008</b>	0.386 ± 0.009	0.340 ± 0.022	0.275 ± 0.015	0.323 ± 0.016
Solar	0.05	<b>0.095 ± 0.015</b>	<u>0.142 ± 0.016</u>	0.165 ± 0.014	0.291 ± 0.009	0.241 ± 0.102	0.339 ± 0.031	0.151 ± 0.017
	0.10	<b>0.083 ± 0.015</b>	<u>0.124 ± 0.018</u>	0.132 ± 0.015	0.276 ± 0.010	0.251 ± 0.081	0.170 ± 0.014	0.128 ± 0.017
	0.20	<b>0.072 ± 0.015</b>	0.108 ± 0.014	0.109 ± 0.012	0.270 ± 0.010	0.314 ± 0.035	<u>0.088 ± 0.010</u>	0.110 ± 0.016
	0.30	<b>0.061 ± 0.012</b>	0.100 ± 0.015	0.098 ± 0.012	0.266 ± 0.010	0.338 ± 0.05	<u>0.063 ± 0.009</u>	0.103 ± 0.017
	0.50	<u>0.054 ± 0.013</u>	0.094 ± 0.013	0.088 ± 0.013	0.262 ± 0.009	0.315 ± 0.080	<b>0.044 ± 0.008</b>	0.096 ± 0.016
Traffic	0.05	<u>0.283 ± 0.016</u>	0.293 ± 0.007	<b>0.261 ± 0.010</b>	0.363 ± 0.007	0.406 ± 0.074	0.813 ± 0.027	0.387 ± 0.014
	0.10	<b>0.211 ± 0.012</b>	<u>0.237 ± 0.006</u>	0.245 ± 0.009	0.362 ± 0.006	0.319 ± 0.025	0.701 ± 0.026	0.293 ± 0.012
	0.20	<b>0.168 ± 0.006</b>	<u>0.197 ± 0.005</u>	0.224 ± 0.008	0.361 ± 0.006	0.270 ± 0.012	0.508 ± 0.022	0.249 ± 0.010
	0.30	<b>0.151 ± 0.007</b>	<u>0.180 ± 0.006</u>	0.197 ± 0.007	0.355 ± 0.006	0.251 ± 0.006	0.387 ± 0.018	0.228 ± 0.009
	0.50	<b>0.139 ± 0.007</b>	<u>0.160 ± 0.008</u>	0.161 ± 0.060	0.354 ± 0.007	0.278 ± 0.040	0.263 ± 0.013	0.204 ± 0.009

**Baselines** To assess the effectiveness of our approach, we perform a comparison with various baselines, which are detailed in Section 2. We include SOTA imputation methods such as SAITS, BRITS, and TIDER, and an advanced interpolation method for irregularly sampled time series, mTAN. In addition, we include two classic machine learning baselines, K-Nearest Neighbours (KNN) and linear interpolation, which are valuable for getting an insight into the complexity of the problem. We evaluate the performance of these methods on the three datasets mentioned above. For each dataset, we divide the data into five independent periods of about three months each (2000 time steps for *Electricity* and *Traffic*, and 10,000 time steps for *Solar*) to obtain robust results over one year. We evaluate the quality of the models for different subsampling rates, ranging from the easiest one  $\tau = 0.5$  to the most difficult one  $\tau = 0.05$ .

**Results** We show in Table 1 that, TimeFlow consistently outperforms other models across all subsampling rates for the given datasets despite a few exceptions. The improvements range from 10% to 50%, especially for low sampling rates. Qualitatively, we see in Figure 2 that our model shows impressive imputation capabilities. It manages to capture well the different frequencies and amplitudes in a moderately difficult case (for sample 35) while preventing extra high frequencies and the underestimation of the amplitude of some peaks. In the more challenging case (sample 25), where the series behave atypically due to internal value and frequency variations, TimeFlow imputes correctly at most timestamps, better than BRITS, the best baseline.

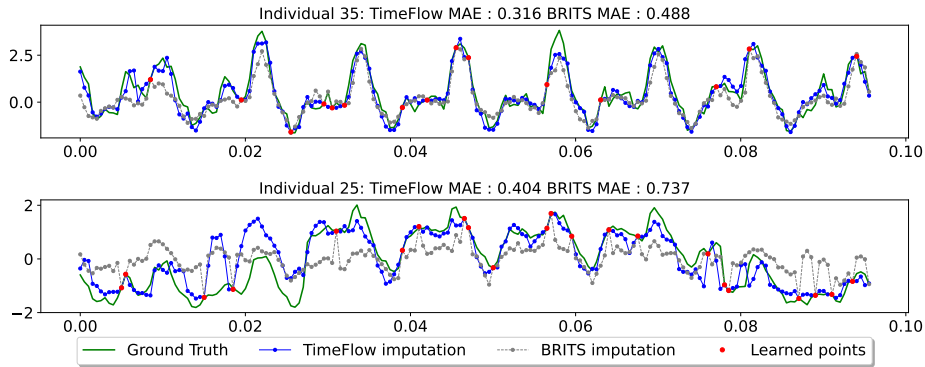


Figure 2: *Electricity* dataset. TimeFlow imputation (blue line) and BRITS imputation (gray line) with 10% of known point (red points) on the eight first days of samples 35 (top) and 25 (bottom).

**New samples and new periods** While imputing missing values for a fixed set of known samples is helpful, it is also crucial to infer new samples in an unseen period, often encountered in practical applications (e.g., new sensor installations). Deep learning SOTA methods require retraining the entire model when imputing new samples, whereas our model quickly adapts to new samples and/or unseen periods, thanks to the efficient adaptation in the latent space. In additional experiments, our model achieves comparable imputation results for both new samples and known samples in new time windows. We provide the results of these experiments in the supplementary material.

## 4.2 Forecasting

In this section, we consider the forecasting task, which is the most prevalent task in time series analysis.

### 4.2.1 Forecasting for known samples

In this scenario, we are interested in the conventional long-term forecasting scenario. It consists in predicting the phenomenon in a specific future period, i.e., horizon, based on the history of a limited past period, i.e., a look-back window. The forecaster is trained on a set of  $n$  observed samples and tested on new periods for the same samples.

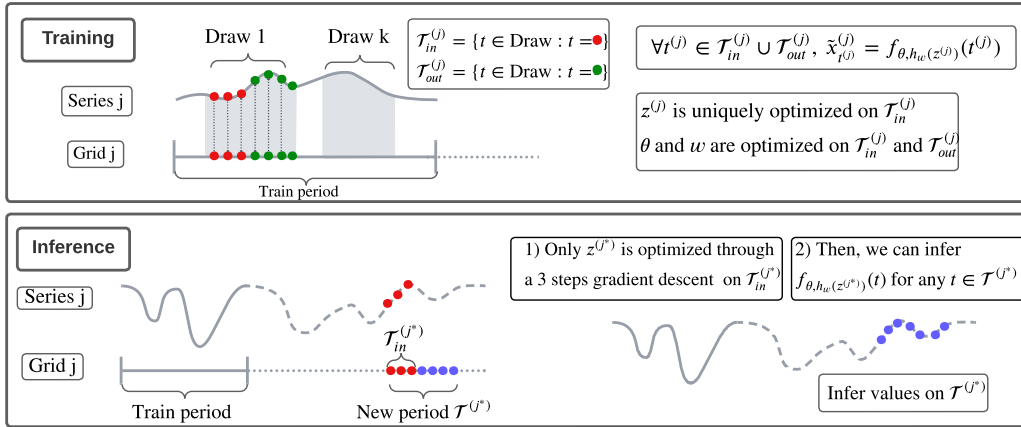


Figure 3: Training and inference procedures for forecasting for known samples

**Setting** For a given time series  $x^{(j)}$ ,  $\mathcal{T}_{in}^{(j)}$  denotes the look-back window of  $L$  points and  $\mathcal{T}_{out}^{(j)}$  the horizon of  $H$  points. During training, at each epoch, we randomly draw several pairs of look-back windows and horizon  $(\mathcal{T}_{in}^{(j)} \cup \mathcal{T}_{out}^{(j)})_{j \in \mathcal{B}}$ . The codes and parameters  $z^{(j)}$ ,  $\theta$ ,  $w$  are then optimized on these windows according to Algorithm 1. During inference for unseen periods  $\mathcal{T}^{(j^*)}$ , the parameters of the INR and the hypernetwork  $\theta$ ,  $w$  are fixed, and the code  $z^{(j^*)}$  is optimized on the look-back window  $\mathcal{T}_{in}^{(j^*)}$  through the  $K$ -step gradient descent process. Then we can infer within both the look-back window and the horizon for any time step. The whole procedure is illustrated in Figure 3.

**Baselines** In order to evaluate the quality of our model in long-term forecasting, we compare to the SOTA baselines presented in Section 2: PatchTST, DLinear, DeepTime, AutoFormer, and Informer. We include the heuristic baseline Repeat, which repeats the last observed window to predict in the horizon. It should be noted that Repeat may perform well only when the look-back window coincides with the seasonality. Thus, the Repeat baseline should be seen as an indicative measure. For each dataset, we train the model on a given period and test it on new periods. We present in Table 2 the forecasting results for a look-back window of length 512 and from standard horizons in long-term forecasting:  $H \in \{96, 192, 336, 720\}$ .

**Results** Our approach is in the top two across all datasets and horizons. We show that we are comparable to the current SOTA approach PatchTST with negligible differences. We observe that,

Table 2: Mean MAE forecast results over different time window. H stands for the horizon. Bold results are best, underline results are second best.

	$H$	TimeFlow	Patch-TST	DLinear	DeepTime	AutoFormer	Informer	Repeat
Electricity	96	<u>0.228 ± 0.028</u>	<b>0.221 ± 0.023</b>	0.241 ± 0.030	0.244 ± 0.026	0.546 ± 0.277	0.603 ± 0.255	0.341 ± 0.044
	192	<u>0.238 ± 0.020</u>	<b>0.229 ± 0.020</b>	0.252 ± 0.025	0.252 ± 0.019	0.500 ± 0.190	0.690 ± 0.291	0.318 ± 0.029
	336	<u>0.270 ± 0.031</u>	<b>0.251 ± 0.027</b>	0.288 ± 0.038	0.284 ± 0.034	0.523 ± 0.188	0.736 ± 0.271	0.299 ± 0.036
	720	<u>0.316 ± 0.055</u>	<b>0.297 ± 0.039</b>	0.365 ± 0.059	0.359 ± 0.051	0.631 ± 0.237	0.746 ± 0.265	0.495 ± 0.044
SolarH	96	<b>0.190 ± 0.013</b>	0.262 ± 0.070	0.208 ± 0.014	<u>0.201 ± 0.019</u>	0.245 ± 0.045	0.248 ± 0.022	0.290 ± 0.056
	192	<b>0.202 ± 0.020</b>	0.253 ± 0.051	0.217 ± 0.022	<u>0.204 ± 0.028</u>	0.333 ± 0.107	0.270 ± 0.031	0.212 ± 0.008
	336	0.209 ± 0.017	0.259 ± 0.071	0.217 ± 0.026	<u>0.199 ± 0.026</u>	0.334 ± 0.079	0.328 ± 0.048	<b>0.187 ± 0.015</b>
	720	<b>0.218 ± 0.041</b>	0.267 ± 0.064	0.249 ± 0.034	<u>0.229 ± 0.024</u>	0.351 ± 0.055	0.337 ± 0.037	0.366 ± 0.017
Traffic	96	<u>0.217 ± 0.032</u>	<b>0.203 ± 0.037</b>	0.228 ± 0.033	0.228 ± 0.032	0.319 ± 0.059	0.372 ± 0.078	0.504 ± 0.057
	192	<u>0.212 ± 0.028</u>	<b>0.197 ± 0.030</b>	0.221 ± 0.023	0.220 ± 0.022	0.511 ± 0.247	0.368 ± 0.057	0.347 ± 0.030
	336	<u>0.238 ± 0.034</u>	<b>0.222 ± 0.039</b>	0.250 ± 0.040	0.245 ± 0.038	0.561 ± 0.263	0.434 ± 0.061	0.256 ± 0.048
	720	<u>0.279 ± 0.050</u>	<b>0.269 ± 0.057</b>	0.300 ± 0.057	0.290 ± 0.052	0.638 ± 0.067	0.462 ± 0.062	0.579 ± 0.068

despite comparable results between TimeFlow and the DLinear, DeepTime baselines for the 96, 192, and 336 time horizons, the difference becomes more significant when the longest horizon is considered. Also, AutoFormer and Informer perform poorly. To give an insight into these results, we provide a detailed analysis of their predictions in the supplementary material. The analysis reveals that while these methods produce reasonably accurate forecasts for the immediate horizon after the training period, they struggle to generalize effectively to unseen periods.

**Discussion** The results show that our method consistently performs as well as the leading forecaster, PatchTST, in the setting with evenly distributed time steps. This achievement is significant as our continuous model can achieve the same level of performance as discrete methods within their specific setting.

**New periods and new samples** An important feature of our model is that it uses a shared architecture conditioned by a sample and a period specific vector, which does not directly model the interdependence between samples. Consequently, the trained forecaster for a particular set of samples can be re-used for new individuals across new periods by conditioning the trained architecture with a new code. Unlike Informer, AutoFormer or DLinear architectures, which directly model the relationships between samples, PatchTST considers the independence between channels, which enables it to generalize to new individuals. In the supplementary materials, we demonstrate that our architecture and PatchTST are both able to generalize to new samples, with no significant performance drop compared to the samples seen during training.

#### 4.2.2 Forecasting on new periods for unknown samples with missing values

**Setting** After undergoing training for a specific duration on a given set of samples, our model demonstrates continuity, enabling us to extend its capabilities to model a continuum for new samples across different time windows. To accomplish this, we maintain the same training configuration as described in Section 4.2.1, but apply inference to new samples within unseen time windows.

**Baseline** In the above scenario, models such as PatchTST (and other DL models) must proceed in two steps: (i) completing the look-back window on a dense regular grid using imputation; (ii) apply the model on the completed window to predict the future. We compared TimeFlow with the following two-step processing baseline: linear interpolation handling the missing values within the partially observed look-back window, and PatchTST handling the forecasting task. Due to the unavailability of data from other samples for the same period, when dealing with unseen time windows for new samples, we are restrained to interpolation as imputation method. We conducted experiments on the *Traffic* and *Electricity* datasets, focusing on the 96 and 192 horizons. In Table 3, we present the results at different sampling rates  $\tau \in \{0.5, 0.2, 0.1\}$  within the look-back window.

Table 3: MAE results for forecasting on new samples and new period with missing values in the look-back window. Best results are in bold.

		TimeFlow		Linear interpo + PatchTST		
	H	$\tau$	Imputation error	Forecast error	Imputation error	Forecast error
Electricity	96	0.5	<b>0.184 ± 0.004</b>	<b>0.247 ± 0.024</b>	0.257 ± 0.008	0.279 ± 0.026
		0.2	<b>0.245 ± 0.007</b>	<b>0.275 ± 0.027</b>	0.482 ± 0.019	0.451 ± 0.042
		0.1	<b>0.357 ± 0.016</b>	<b>0.362 ± 0.029</b>	0.663 ± 0.029	0.634 ± 0.053
	192	0.5	<b>0.184 ± 0.005</b>	<b>0.240 ± 0.026</b>	0.258 ± 0.006	0.280 ± 0.032
		0.2	<b>0.250 ± 0.009</b>	<b>0.289 ± 0.029</b>	0.481 ± 0.021	0.450 ± 0.054
		0.1	<b>0.372 ± 0.017</b>	<b>0.388 ± 0.030</b>	0.669 ± 0.030	0.650 ± 0.060
Traffic	96	0.5	<b>0.219 ± 0.017</b>	<b>0.224 ± 0.033</b>	0.276 ± 0.012	0.255 ± 0.041
		0.2	<b>0.278 ± 0.017</b>	<b>0.252 ± 0.029</b>	0.532 ± 0.017	0.483 ± 0.040
		0.1	<b>0.418 ± 0.019</b>	<b>0.382 ± 0.014</b>	0.738 ± 0.023	0.721 ± 0.073
	192	0.5	<b>0.211 ± 0.014</b>	<b>0.216 ± 0.028</b>	0.276 ± 0.011	0.245 ± 0.029
		0.2	<b>0.271 ± 0.017</b>	<b>0.242 ± 0.026</b>	0.532 ± 0.020	0.480 ± 0.050
		0.1	<b>0.397 ± 0.025</b>	<b>0.360 ± 0.022</b>	0.734 ± 0.022	0.787 ± 0.172

**Results** Table 3 shows that our method significantly outperforms the baseline (linear interpolation + PatchTST). This poor performance of the baseline can be attributed to the imputation errors induced by the linear interpolation. Although our method was not explicitly trained for imputation, it demonstrates a remarkable capability to recover the ground truth values for the partially observed historical window, leading to precise forecasts. We show the extended results for *Traffic* and *Electricity* datasets in the supplementary materials. In addition, our method exhibits effectiveness even at significantly low sampling rates. When it comes to the results presented in Table 2, our method shows a relatively modest degradation when the subsampling rate drops, in comparison to the results obtained in the optimal setting. We illustrate the qualitative results in Figure 4 using a look-back window with a 20% sampling rate for a horizon of 96 time steps.

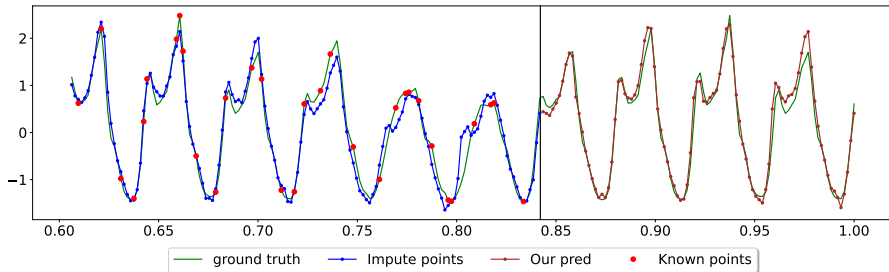


Figure 4: *Traffic dataset, test sample 88*. In this figure, we simultaneously impute and forecast at horizon 96 with a 20% partially observed look back window of length 512.

## 5 Conclusion and Discussion

For the first time, we have introduced a modulated INR architecture that allows continuous time series modeling. Our experiments have demonstrated superior performance compared to SOTA imputation methods, and comparable results to SOTA forecasting methods in the usual settings. Furthermore, the inherent continuity of our approach, combined with the ability to modulate the INR parameters, provides unparalleled flexibility. This versatility allows TimeFlow to effectively address various challenges, including forecasting with missing values, accommodating irregular time steps, and applying the trained model to new samples within different time windows.

In this paper, we focused on the analysis of multi-sample univariate time series. To extend our findings to the multi-sample multivariate case, a simple approach is to modify the output dimension

of the INR network. However, this approach is not applicable to the case where univariate time series for a given sample are observed at different intervals. This is because the INR requires all values at each time step for a given sample. As a result, our current work is unable to effectively handle multi-sample multivariate time series while maintaining all the desired properties of our architecture. Achieving the same flexibility that TimeFlow allows requires further research.

## Acknowledgments

We would like to thank Tahar Nabil for the valuable discussions on this project. We also acknowledge the support of EDF R&D. Finally, we express our gratitude to the contributors who provided the public datasets used in this paper.

## References

- E. D. Brouwer, J. Simm, A. Arany, and Y. Moreau. Gru-ode-bayes: continuous modeling of sporadically-observed time series. In *Proceedings of the 33rd International Conference on Neural Information Processing Systems*, pages 7379–7390, 2019.
- W. Cao, D. Wang, J. Li, H. Zhou, Y. Li, and L. Li. Brits: bidirectional recurrent imputation for time series. In *Proceedings of the 32nd International Conference on Neural Information Processing Systems*, pages 6776–6786, 2018.
- H. Chen, S. Grant-Muller, L. Mussone, and F. Montgomery. A study of hybrid neural network approaches and the effects of missing data on traffic forecasting. *Neural Computing & Applications*, 10:277–286, 2001.
- J. S. Clark and O. N. Bjørnstad. Population time series: process variability, observation errors, missing values, lags, and hidden states. *Ecology*, 85(11):3140–3150, 2004.
- G. Corani, A. Benavoli, and M. Zaffalon. Time series forecasting with gaussian processes needs priors. In *Machine Learning and Knowledge Discovery in Databases. Applied Data Science Track: European Conference, ECML PKDD 2021, Bilbao, Spain, September 13–17, 2021, Proceedings, Part IV 21*, pages 103–117. Springer, 2021.
- W. Du, D. Côté, and Y. Liu. Saits: Self-attention-based imputation for time series. *Expert Systems with Applications*, 219:119619, 2023.
- E. Dupont, H. Kim, S. M. A. Eslami, D. J. Rezende, and D. Rosenbaum. From data to functa: Your data point is a function and you can treat it like one. In *International Conference on Machine Learning, ICML 2022, 17-23 July 2022, Baltimore, Maryland, USA*, volume 162 of *Proceedings of Machine Learning Research*, pages 5694–5725. PMLR, 2022.
- R. Fathony, A. K. Sahu, D. Willmott, and J. Z. Kolter. Multiplicative filter networks. In *International Conference on Learning Representations*, 2021.
- E. Fons, A. Sztrajman, Y. El-Laham, A. Iosifidis, and S. Vyetrenko. Hypertime: Implicit neural representation for time series. *CoRR*, abs/2208.05836, 2022.
- V. Fortuin, D. Baranchuk, G. Rätsch, and S. Mandt. Gp-vae: Deep probabilistic time series imputation. In *International conference on artificial intelligence and statistics*, pages 1651–1661. PMLR, 2020.
- L. Huang and T. Hoefler. Compressing multidimensional weather and climate data into neural networks. In *International Conference on Learning Representations, ICLR, 2023*.
- K. Jeong and Y. Shin. Time-series anomaly detection with implicit neural representation. *CoRR*, abs/2201.11950, 2022.
- T. Kim, W. Ko, and J. Kim. Analysis and impact evaluation of missing data imputation in day-ahead pv generation forecasting. *Applied Sciences*, 9(1):204, 2019.
- S. Liu, H. Yu, C. Liao, J. Li, W. Lin, A. X. Liu, and S. Dustdar. Pyraformer: Low-complexity pyramidal attention for long-range time series modeling and forecasting. In *The Tenth International Conference on Learning Representations, ICLR 2022, Virtual Event, April 25-29, 2022, 2022*.
- S. Liu, X. Li, G. Cong, Y. Chen, and Y. Jiang. Multivariate time-series imputation with disentangled temporal representations. In *The Eleventh International Conference on Learning Representations, ICLR, 2023*.

- Y. Liu, R. Yu, S. Zheng, E. Zhan, and Y. Yue. Naomi: Non-autoregressive multiresolution sequence imputation. *Advances in neural information processing systems*, 32, 2019.
- Y. Luo, X. Cai, Y. Zhang, J. Xu, et al. Multivariate time series imputation with generative adversarial networks. *Advances in neural information processing systems*, 31, 2018.
- Y. Luo, Y. Zhang, X. Cai, and X. Yuan. E2gan: End-to-end generative adversarial network for multivariate time series imputation. In *Proceedings of the 28th international joint conference on artificial intelligence*, pages 3094–3100. AAAI Press, 2019.
- B. Mildenhall, P. P. Srinivasan, M. Tancik, J. T. Barron, R. Ramamoorthi, and R. Ng. Nerf: Representing scenes as neural radiance fields for view synthesis. *Communications of the ACM*, 65(1): 99–106, 2021.
- Y. Nie, N. H. Nguyen, P. Sinthong, and J. Kalagnanam. A time series is worth 64 words: Long-term forecasting with transformers. *CoRR*, abs/2211.14730, 2022.
- C. E. Rasmussen and C. K. I. Williams. *Gaussian processes for machine learning*. Adaptive computation and machine learning. MIT Press, 2006.
- Y. Rubanova, R. T. Q. Chen, and D. Duvenaud. Latent odes for irregularly-sampled time series. *CoRR*, abs/1907.03907, 2019.
- M. Schulz and K. Stattegger. Spectrum: Spectral analysis of unevenly spaced paleoclimatic time series. *Computers & Geosciences*, 23(9):929–945, 1997.
- S. N. Shukla and B. M. Marlin. Multi-time attention networks for irregularly sampled time series. In *9th International Conference on Learning Representations, ICLR 2021, Virtual Event, Austria, May 3-7, 2021*, 2021.
- V. Sitzmann, J. N. P. Martel, A. W. Bergman, D. B. Lindell, and G. Wetzstein. Implicit neural representations with periodic activation functions. In *Advances in Neural Information Processing Systems 33: Annual Conference on Neural Information Processing Systems 2020, NeurIPS 2020, December 6-12, 2020, virtual*, 2020.
- M. Tancik, P. Srinivasan, B. Mildenhall, S. Fridovich-Keil, N. Raghavan, U. Singhal, R. Ramamoorthi, J. Barron, and R. Ng. Fourier features let networks learn high frequency functions in low dimensional domains. *Advances in Neural Information Processing Systems*, 33:7537–7547, 2020.
- Y. Tashiro, J. Song, Y. Song, and S. Ermon. Csd: Conditional score-based diffusion models for probabilistic time series imputation. *Advances in Neural Information Processing Systems*, 34: 24804–24816, 2021.
- S. J. Taylor and B. Letham. Forecasting at scale. *PeerJ Prepr.*, 5:e3190, 2017.
- G. Woo, C. Liu, D. Sahoo, A. Kumar, and S. C. H. Hoi. Deeptime: Deep time-index meta-learning for non-stationary time-series forecasting. *CoRR*, abs/2207.06046, 2022.
- H. Wu, J. Xu, J. Wang, and M. Long. Autoformer: Decomposition transformers with auto-correlation for long-term series forecasting. In M. Ranzato, A. Beygelzimer, Y. N. Dauphin, P. Liang, and J. W. Vaughan, editors, *Advances in Neural Information Processing Systems 34: Annual Conference on Neural Information Processing Systems 2021, NeurIPS 2021, December 6-14, 2021, virtual*, pages 22419–22430, 2021.
- Y. Yin, M. Kirchmeyer, J.-Y. Franceschi, A. Rakotomamonjy, and P. Gallinari. Continuous pde dynamics forecasting with implicit neural representations. In *International Conference on Learning Representations, ICLR*, 2023.
- A. Zeng, M. Chen, L. Zhang, and Q. Xu. Are transformers effective for time series forecasting? *CoRR*, abs/2205.13504, 2022.
- H. Zhou, S. Zhang, J. Peng, S. Zhang, J. Li, H. Xiong, and W. Zhang. Informer: Beyond efficient transformer for long sequence time-series forecasting. In *Proceedings of the AAAI conference on artificial intelligence*, pages 11106–11115, 2021.
- T. Zhou, Z. Ma, Q. Wen, X. Wang, L. Sun, and R. Jin. Fedformer: Frequency enhanced decomposed transformer for long-term series forecasting. In K. Chaudhuri, S. Jegelka, L. Song, C. Szepesvári, G. Niu, and S. Sabato, editors, *International Conference on Machine Learning, ICML 2022, 17-23 July 2022, Baltimore, Maryland, USA*, volume 162 of *Proceedings of Machine Learning Research*, pages 27268–27286. PMLR, 2022.
- L. Zintgraf, K. Shiarli, V. Kurin, K. Hofmann, and S. Whiteson. Fast context adaptation via meta-learning. In *International Conference on Machine Learning*, pages 7693–7702. PMLR, 2019.

## A Architecture details and ablation studies

### A.1 Architecture details

#### A.1.1 Overview

Section 3 introduced a flexible modulated INR architecture designed to perform imputation and forecasting tasks. We present in Figure 5 a schematic version of this architecture.

We used NVIDIA TITAN RTX 12Go single GPUs to conduct all the experiments for our method, which is coded in PyTorch (Python 3.9.2).

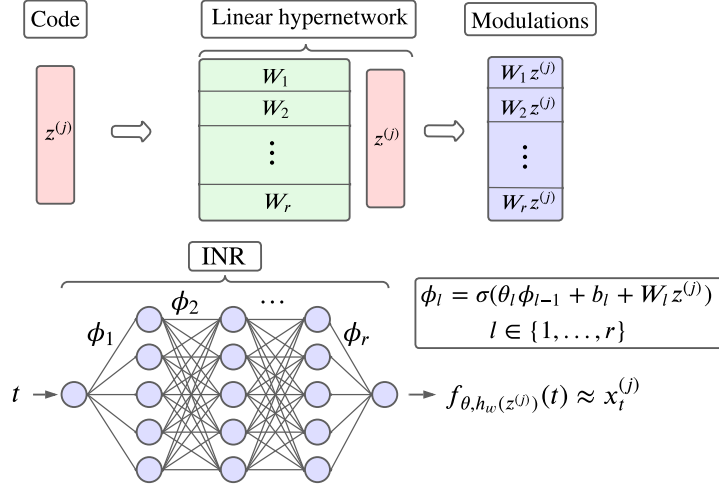


Figure 5: Architecture overview.  $\sigma$  stands for a point-wise activation function

#### A.1.2 Fourier features network

There are several options for the architecture of the INR. We choose a Fourier features network, which is an MLP with ReLU activations, accompanied by a frequency-based embedding for the input coordinates, as in [Tancik et al. \(2020\)](#); [Mildenhall et al. \(2021\)](#). Namely for a time coordinate  $t \in [0, 1]$ , the output of the INR  $f_\theta$  is given by  $f_\theta(t) = \text{MLP}(\gamma(t))$ , where  $\gamma$  is a frequency embedding and a ReLU activation function is used. In our case, we choose  $\gamma(t) := (\sin(\pi t), \cos(\pi t), \dots, \sin(2^N \pi t), \cos(2^N \pi t))$ , with  $N$  the number of frequencies. This architecture, despite its simplicity, outperformed other common INR architectures (e.g. [Sitzmann et al. \(2020\)](#)) on the aforementioned tasks such as time-series reconstruction, imputation and forecasting. We hypothesize that the MLP with ReLU activations correctly learns the different frequencies of time series with multi-temporal patterns by switching on or off the Fourier embedding frequencies.

#### A.1.3 Hyperparameters

For all imputation and forecasting experiments we choose the following hyperparameters :

- $z$  dimension: 128
- Number of layers: 7
- Hidden layers dimension: 256
- $\gamma(t) \in \mathbb{R}^{2 \times 64}$
- $z$  code learning rate ( $\alpha$  in Equation (1)):  $10^{-2}$
- Hypernetwork and INR learning rate:  $5 \times 10^{-4}$
- Number of steps in inner loop:  $K = 3$
- Number of epochs:  $4 \times 10^4$
- Batch size: 64

It is worth noting that the hyperparameters mentioned above remain consistent across all experiments conducted in the paper. We chose to maintain a fixed set of hyperparameters for our model, while other imputation and forecasting approaches commonly fine-tune hyperparameters based on a validation dataset. The obtained results exhibit high robustness across various settings, suggesting that the selected hyperparameters are already effective in achieving reliable outcomes.

## A.2 Ablation studies

### A.2.1 Ablation study: Fourier features vs SIREN on imputation task

**Baseline** The SIREN network differs from the Fourier features network because it does not explicitly incorporate frequencies as input. Instead, it is a multi-layer perceptron network that utilizes sine activation functions. An adjustable parameter, denoted  $\omega_0$ , is multiplied with the input matrices of the preceding layers to capture a broader range of frequencies. For this comparison, we adopt the same hyperparameters described in Appendix A.1.3, selecting  $\omega_0 = 30$  to align with [Sitzmann et al. \(2020\)](#). Furthermore, we set the learning rate of both the hypernetwork and the INR to  $5 \times 10^{-5}$  to enhance training stability. In Table 4, we compare the imputation results obtained by the Fourier features network and the SIREN network, specifically focusing on the first period of size 2000 from the *Electricity* dataset.

Table 4: MAE imputation errors on the first time window of *Electricity* dataset. Best results are bold.

	$\tau$	Fourier features	SIREN
	0.05	<b>0.323</b>	0.466
	0.10	<b>0.252</b>	0.350
Electricity	0.20	<b>0.224</b>	0.242
	0.30	<b>0.211</b>	0.222
	0.50	<b>0.194</b>	0.209

**Results** According to the results presented in Table 4, the Fourier features network outperforms the SIREN network in the imputation task on the *Electricity* dataset. Notably, the performance gap between the two network architectures are more pronounced at low sampling rates. This disparity can be attributed to the SIREN network’s difficulty in accurately capturing high frequencies when the time series is sparsely observed.

### A.2.2 Ablation study on $z$ dimension

The dimension of the latent codes  $z$  is a crucial parameter in our architecture. If it is too small, it limits individual contribution from the time series, resulting in a poorer curve fit. Consequently, this adversely affects the performance of both the imputation and forecasting tasks. On the other hand, if the dimension of  $z$  is excessively large, it can lead to overfitting, hindering the model’s ability to generalize to new data points.

**Baselines** To investigate the impact of  $z$  dimensionality on the performance of the INR, we conducted experiments on the *Electricity* dataset, specifically focusing on the imputation task. We varied the sizes of  $z$  within  $\{32, 64, 128, 256\}$ . The other hyperparameters are set as presented in Appendix A.1.3. The obtained results for each  $z$  dimension are summarized in Table 5.

**Results** The results presented in Table 5 highlight the importance of the  $z$ -dimension, as it significantly impacts the results. We found that a dimension of 128 was a suitable compromise for all our experiments.

### A.2.3 Discussion on other hyperparameters

While the dimension of  $z$  is indeed a crucial hyperparameter, it is important to note that other hyperparameters also play a significant role in the performance of the INR. For example, the number

Table 5: MAE imputation errors on the first time window of *Electricity* dataset. Best results are bold.

	$\tau$	$\dim(z) = 32$	$\dim(z) = 64$	$\dim(z) = 128$	$\dim(z) = 256$
Electricity	0.05	0.370	0.364	<b>0.323</b>	0.354
	0.10	0.302	0.301	<b>0.252</b>	0.283
	0.20	0.269	0.265	<b>0.224</b>	0.247
	0.30	0.242	0.245	<b>0.211</b>	0.238
	0.50	0.224	0.240	<b>0.194</b>	0.217

of layers in the MLP directly affects the ability of the model to fit the time series. In our experiments, we have observed that using five or more layers yields good performance, and including additional layers can lead to slight improvements in the generalization settings.

Similarly, the number of frequencies used in the input to the Fourier function network is another important hyperparameter. Using too few frequencies can limit the network’s ability to capture patterns, while using too many frequencies can hinder its ability to generalize accurately.

The choice of learning rate is critical for achieving stable convergence during training. Therefore, in practice, we use a low learning rate combined with a cosine annealing scheduler to ensure stable and effective training.

## B Datasets and normalization

**Datasets information** Table 6 provides a concise overview of the main information about the datasets used for forecasting and imputation tasks.

Table 6: Summary of datasets information

Dataset name	Number of samples	Number of time steps	Sampling frequency	Location	Years
Electricity	321	26 304	hourly	Portugal	2012 – 2014
Traffic	862	17 544	hourly	San Francisco bay	2015 – 2016
Solar	137	52 560	10 minutes	Alabama	2006
SolarH	137	8 760	hourly	Alabama	2006

**z-normalization** To preprocess each dataset, we apply the widely used z-normalization technique per-sample  $j$  on the entire series:  $x_{norm}^{(j)} = \frac{x^{(j)} - \text{mean}(x^{(j)})}{\text{std}(x^{(j)})}$ .

Additionally, during the imputation training phase, we employ batch normalization, but we do not utilize it during the forecasting training phase.

## C Imputation experiments

### C.1 Models complexity

We can see in Table 7 that our method has fewer parameters than SOTA imputation methods, 10 times less than BRITS and 20 times less than SAITS. It is mainly due to their modelisation of interaction between samples. SAITS, which is based on transformers has the highest number of parameters when mTAN has the lowest number of parameters.

Table 7: Number of parameters for each DL methods on the imputation task on the *Electricity* dataset.

	TimeFlow	SAITS	BRITS	TIDER	mTAN
Number of parameters	602k	11 137k	6 220k	1 034k	113k

## C.2 Impute for new sample on new period

**Setting** In this section we analyze in details the results obtained from the setting described at the end of Section 4.1. Specifically, TimeFlow is trained on a given set of samples within a defined time window and then used for inference on a new time windows for different samples. The training and inference processes are illustrated visually in Figure 6.

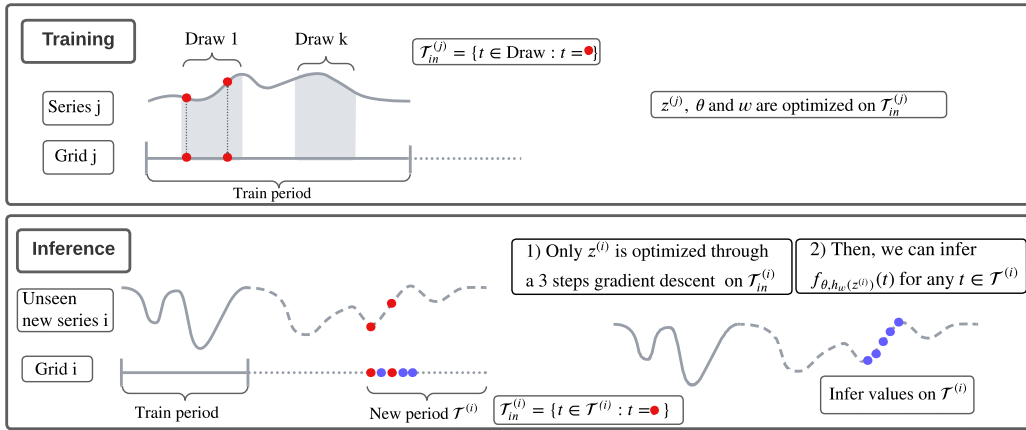


Figure 6: Training and inference procedures for imputation for new samples on new periods

**Baseline** In this setting, data from other samples for the same period is not available when dealing with unseen time windows for new samples. We are then restrained to interpolation as an imputation method when dealing with unseen time windows for new samples.

**Results** We can see in Table 8 that our method is stable for new samples across the different datasets and sampling rates. Experimentally, our method is able to generalize to new samples for the imputation task. Note that the results presented here are not as good as the ones presented in Table 1. This is expected since we evaluate TimeFlow on unseen time windows, as opposed to fixed time windows in the usual imputation setting.

Table 8: MAE imputation errors results for imputation on new windows

	$\tau$	Known samples		New samples	
		TimeFlow	Linear interpo	TimeFlow	Linear interpo
Electricity	0.05	0.519 ± 0.029	0.831 ± 0.048	0.530 ± 0.044	0.846 ± 0.065
	0.10	0.408 ± 0.022	0.714 ± 0.041	0.418 ± 0.036	0.729 ± 0.059
	0.20	0.334 ± 0.018	0.516 ± 0.027	0.327 ± 0.030	0.528 ± .044
	0.30	0.283 ± 0.013	0.392 ± 0.020	0.292 ± 0.027	0.403 ± 0.034
	0.50	0.256 ± 0.011	0.272 ± 0.012	0.264 ± 0.025	0.280 ± 0.022
Traffic	0.05	0.509 ± 0.031	0.799 ± 0.049	0.501 ± 0.025	0.800 ± 0.034
	0.10	0.421 ± 0.024	0.691 ± 0.045	0.411 ± 0.019	0.689 ± 0.032
	0.20	0.362 ± 0.020	0.503 ± 0.036	0.351 ± 0.015	0.494 ± 0.025
	0.30	0.337 ± 0.018	0.385 ± 0.029	0.326 ± 0.014	0.374 ± 0.021
	0.50	0.314 ± 0.017	0.262 ± 0.020	0.303 ± 0.013	0.252 ± 0.015
Solar	0.05	0.220 ± 0.018	0.344 ± 0.034	0.219 ± 0.020	0.346 ± 0.033
	0.10	0.155 ± 0.014	0.173 ± 0.014	0.155 ± 0.016	0.174 ± 0.015
	0.20	0.123 ± 0.013	0.090 ± 0.010	0.123 ± 0.013	0.091 ± 0.010
	0.30	0.114 ± 0.012	0.064 ± 0.009	0.114 ± 0.012	0.066 ± 0.008
	0.50	0.108 ± 0.012	0.044 ± 0.008	0.108 ± 0.012	0.045 ± 0.007

## D Forecasting experiments

### D.1 Classic Forecasting setting

#### D.1.1 Distinction between adjacent time windows and new time windows during inference

In Section 4.2.1, we presented the forecasting results for periods outside the training period. These periods can be classified into two types: adjacent to or disjoint from the training period. Figure 7 illustrates these distinct test periods for the *Electricity* dataset. The same principle applies to the *Traffic* and *SolarH* datasets, with one notable difference: the number of test periods is smaller in these datasets compared to *Electricity* dataset due to the fewer time steps available.

In Table 2, we presented the results indistinctly for the two types of test periods: adjacent to and disjoint from the training window. Here, we aim to differentiate the results for these two types of window and emphasize their significant impact on Informer and AutoFormer results. Specifically, Table 9 showcases the results for the test periods adjacent to the training window. In contrast, Table 10 displays the results for the test periods disjointed from the training window

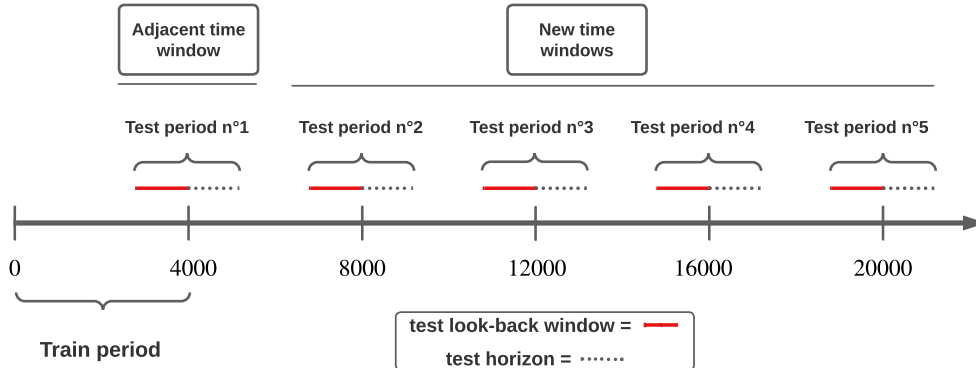


Figure 7: Distinction between adjacent time windows and new time windows during inference for the *Electricity* dataset

**Results** TimeFlow, PatchTST, DLinear and DeepTime maintain consistent forecasting results whether tested on the period adjacent to the training period or on a disjoint period. However, AutoFormer and Informer show a significant drop in performance when tested on new disjoint periods.

Table 9: Mean MAE forecast results for adjacent time windows. H stands for the horizon. Bold results are best, underline results are second best.

	H	TimeFlow	Patch-TST	DLinear	DeepTime	AutoFormer	Informer	Repeat
Electricity	96	<u>0.218 ± 0.017</u>	<b>0.214 ± 0.020</b>	0.236 ± 0.035	0.240 ± 0.027	0.310 ± 0.031	0.293 ± 0.0184	0.341 ± 0.044
	192	<u>0.238 ± 0.012</u>	<b>0.225 ± 0.017</b>	0.248 ± 0.032	0.251 ± 0.023	0.322 ± 0.046	0.336 ± 0.032	0.318 ± 0.029
	336	<u>0.265 ± 0.036</u>	<b>0.242 ± 0.024</b>	0.284 ± 0.043	0.290 ± 0.034	0.330 ± 0.019	0.405 ± 0.044	0.299 ± 0.036
	720	<u>0.318 ± 0.073</u>	<b>0.291 ± 0.040</b>	0.370 ± 0.086	0.356 ± 0.060	0.456 ± 0.052	0.489 ± 0.072	0.495 ± 0.044
SolarH	96	<b>0.172 ± 0.017</b>	0.232 ± 0.008	0.204 ± 0.002	<u>0.197 ± 0.002</u>	0.261 ± 0.053	0.273 ± 0.023	0.290 ± 0.056
	192	<b>0.198 ± 0.010</b>	0.231 ± 0.027	0.211 ± 0.012	<u>0.202 ± 0.014</u>	0.312 ± 0.085	0.256 ± 0.026	0.212 ± 0.008
	336	0.207 ± 0.019	0.254 ± 0.048	0.212 ± 0.019	<u>0.200 ± 0.012</u>	0.341 ± 0.107	0.287 ± 0.006	<b>0.187 ± 0.015</b>
	720	<b>0.215 ± 0.016</b>	0.271 ± 0.036	0.246 ± 0.015	<u>0.240 ± 0.011</u>	0.368 ± 0.006	0.341 ± 0.049	0.366 ± 0.017
Traffic	96	<u>0.216 ± 0.033</u>	<b>0.201 ± 0.031</b>	0.225 ± 0.034	0.229 ± 0.032	0.299 ± 0.080	0.324 ± 0.113	0.504 ± 0.057
	192	<u>0.208 ± 0.021</u>	<b>0.195 ± 0.024</b>	0.215 ± 0.022	0.220 ± 0.020	0.320 ± 0.036	0.321 ± 0.052	0.347 ± 0.030
	336	<u>0.237 ± 0.040</u>	<b>0.220 ± 0.036</b>	0.244 ± 0.035	0.247 ± 0.033	0.450 ± 0.127	0.394 ± 0.066	0.256 ± 0.048
	720	<b>0.266 ± 0.048</b>	<u>0.268 ± 0.050</u>	0.290 ± 0.047	0.290 ± 0.045	0.630 ± 0.043	0.441 ± 0.055	0.579 ± 0.068

Table 10: Mean MAE forecast results for new time windows. H stands for the horizon. Bold results are best, underline results are second best.

	H	TimeFlow	Patch-TST	DLinear	DeepTime	AutoFormer	Informer	Repeat
Electricity	96	<u>0.230 ± 0.012</u>	<b>0.222 ± 0.023</b>	0.240 ± 0.025	0.245 ± 0.026	0.606 ± 0.281	0.605 ± 0.227	0.341 ± 0.044
	192	<u>0.246 ± 0.025</u>	<b>0.231 ± 0.020</b>	0.257 ± 0.027	0.252 ± 0.018	0.545 ± 0.186	0.776 ± 0.257	0.318 ± 0.029
	336	<u>0.271 ± 0.029</u>	<b>0.253 ± 0.027</b>	0.298 ± 0.051	0.285 ± 0.034	0.571 ± 0.181	0.823 ± 0.241	0.299 ± 0.036
	720	<u>0.316 ± 0.051</u>	<b>0.299 ± 0.038</b>	0.373 ± 0.075	0.359 ± 0.048	0.674 ± 0.245	0.811 ± 0.257	0.495 ± 0.044
SolarH	96	<u>0.208 ± 0.005</u>	0.293 ± 0.089	0.212 ± 0.019	<b>0.206 ± 0.026</b>	0.228 ± 0.027	0.234 ± 0.011	0.290 ± 0.056
	192	<b>0.206 ± 0.012</b>	0.274 ± 0.060	0.223 ± 0.029	<u>0.207 ± 0.037</u>	0.356 ± 0.122	0.280 ± 0.033	0.212 ± 0.008
	336	0.211 ± 0.005	0.264 ± 0.088	0.223 ± 0.032	<u>0.199 ± 0.035</u>	0.327 ± 0.029	0.366 ± 0.039	<b>0.187 ± 0.015</b>
	720	<b>0.222 ± 0.020</b>	0.262 ± 0.083	0.251 ± 0.047	<u>0.217 ± 0.028</u>	0.335 ± 0.075	0.333 ± 0.012	0.366 ± 0.017
Traffic	96	<u>0.218 ± 0.042</u>	<b>0.204 ± 0.039</b>	0.229 ± 0.032	0.2285 ± 0.032	0.326 ± 0.049	0.388 ± 0.055	0.504 ± 0.057
	192	<u>0.213 ± 0.028</u>	<b>0.198 ± 0.031</b>	0.223 ± 0.023	0.220 ± 0.023	0.575 ± 0.254	0.381 ± 0.049	0.347 ± 0.030
	336	<u>0.239 ± 0.035</u>	<b>0.223 ± 0.040</b>	0.252 ± 0.042	0.244 ± 0.040	0.598 ± 0.286	0.448 ± 0.055	0.256 ± 0.048
	720	<u>0.280 ± 0.047</u>	<b>0.270 ± 0.059</b>	0.304 ± 0.061	0.290 ± 0.055	0.641 ± 0.072	0.468 ± 0.064	0.579 ± 0.068

### D.1.2 Plots comparison: TimeFlow vs PatchTST

Table 2 demonstrates the similar forecasting performance of TimeFlow and PatchTST across all horizons. To visually represent their predictions, the figures below showcase the forecasted outcomes of these methods for two samples (24 and 38) and two horizons (96 and 192) on the *Electricity*, *SolarH*, and *Traffic* datasets.

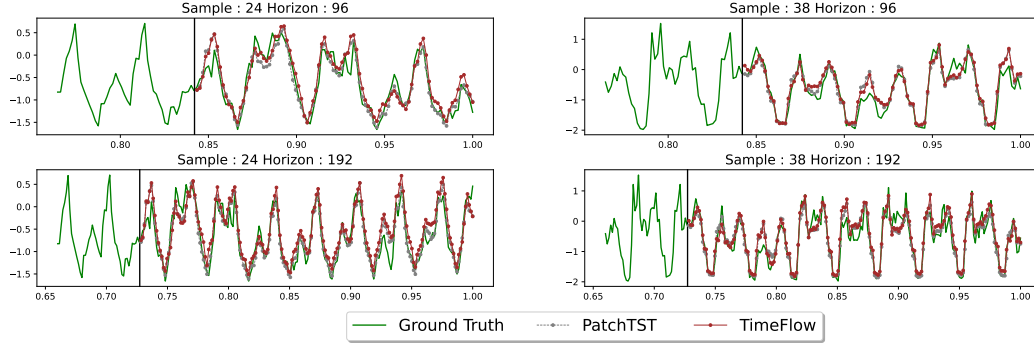


Figure 8: *Electricity* dataset

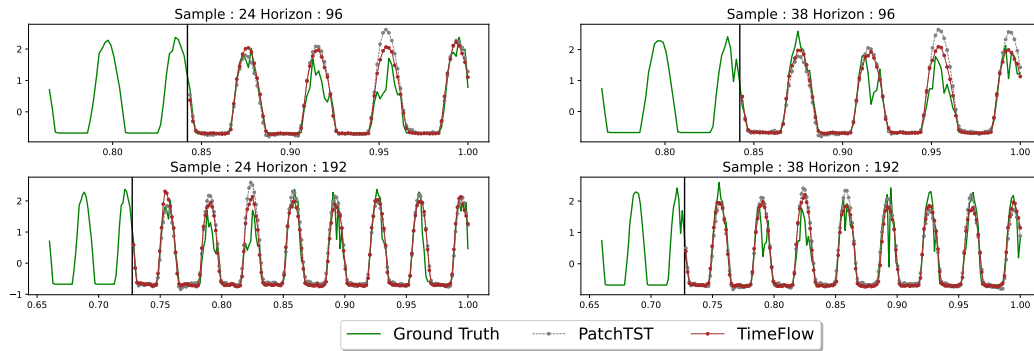


Figure 9: *SolarH* dataset

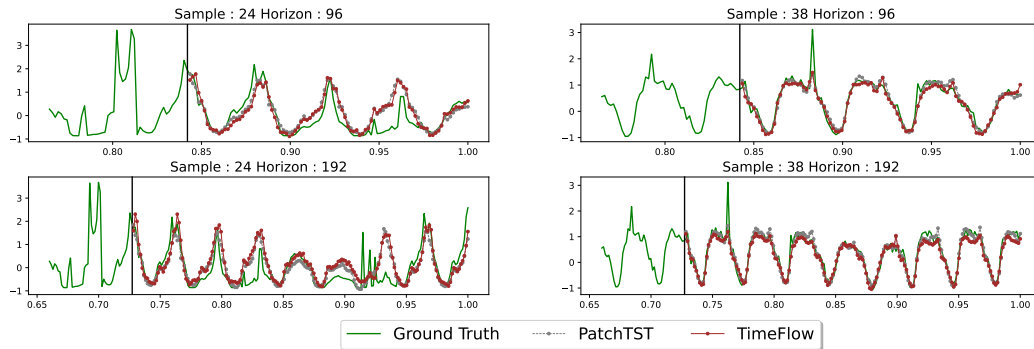


Figure 10: *Traffic* dataset

**Results** The visual analysis of the figures above reveals that the predictions of TimeFlow and PatchTST are remarkably similar. For instance, when examining sample 24 and horizon 192 of the *Traffic* dataset, both forecasters exhibit similar error patterns. The only noticeable distinction emerges in the *SolarH* dataset, where PatchTST tends to overestimate certain peaks.

### D.1.3 Models complexity

In this section, we present the parameter counts for the main forecasting baselines. Except for TimeFlow and DeepTime, the number of parameters varies with the number of samples, the look-back window, and the horizon. Thus, we report the number of parameters for two specific configurations, including a fixed dataset, a fixed look-back window, and a fixed horizon. In Table 11 we see that for PatchTST and DLinear, the larger the horizon, the more the number of parameters increases.

Table 11: The number of parameters for main baselines on the forecasting task on the *Electricity* dataset for horizons 96 and 720. The look-back window size is 512. For DeepTime, we only report the number of parameters for the INR.

	TimeFlow	Patch-TST	DLinear	DeepTime*
96	602k	1 194k	98k	1 315k
720	602k	6 306k	739k	1 315k

## D.2 Forecasting for new samples on new periods

**Setting and baseline** As mentioned in Section 4.2, most forecasters explicitly model the dependencies between samples, which limits their ability to generalize to new samples without retraining the entire model. However, TimeFlow, PatchTST, and DeepTime have the advantage of being reusable for new samples. In Table 12, we present the results of TimeFlow and PatchTST for new periods, considering both known samples and new samples.

Table 12: MAE forecast results for new samples

	H	Known samples		New samples	
		TimeFlow MAE error	PatchTST MAE error	TimeFlow MAE error	PatchTST MAE error
Electricity	96	0.228 ± 0.023	0.211 ± 0.007	0.241 ± 0.023	0.224 ± 0.020
	192	0.244 ± 0.022	0.225 ± 0.014	0.254 ± 0.024	0.238 ± 0.024
	336	0.269 ± 0.036	0.267 ± 0.019	0.277 ± 0.033	0.285 ± 0.005
	720	0.331 ± 0.058	0.310 ± 0.026	0.333 ± 0.059	0.331 ± 0.045
Traffic	96	0.226 ± 0.035	0.208 ± 0.036	0.222 ± 0.031	0.203 ± 0.037
	192	0.217 ± 0.028	0.202 ± 0.029	0.215 ± 0.026	0.199 ± 0.030
	336	0.242 ± 0.036	0.228 ± 0.041	0.240 ± 0.031	0.224 ± 0.036
	720	0.283 ± 0.053	0.275 ± 0.059	0.283 ± 0.049	0.272 ± 0.055
SolarH	96	0.237 ± 0.077	0.256 ± 0.055	0.236 ± 0.081	0.256 ± 0.062
	192	0.238 ± 0.051	0.251 ± 0.239	0.239 ± 0.058	0.250 ± 0.050
	336	0.220 ± 0.027	0.255 ± 0.663	0.220 ± 0.034	0.255 ± 0.066
	720	0.240 ± 0.039	0.267 ± 0.062	0.240 ± 0.042	0.267 ± 0.063

**Results** Table 12 demonstrates the good adaptability of both methods to new samples, as the difference in MAE between known and new samples is marginal.

## D.3 Full forecasting results with missing values

In Section 4.2.2, we presented the forecast results using various sparse look-back windows. In Table 13, we present the same results but with the additional setting  $\tau = 1$ , corresponding to a dense look-back window.

**Results** Although PatchTST performs slightly better with a dense look-back window, its performance significantly deteriorates as the value of  $\tau$  decreases. In contrast, the performance of TimeFlow is only minimally affected by the reduction in the sampling rate.

Table 13: MAE results for forecasting on new samples and new period with missing values in the look-back window. Best results are in bold.

H	$\tau$	TimeFlow		Linear interpo + PatchTST		
		Imputation error	Forecast error	Imputation error	Forecast error	
Electricity	96	1.	0.000 $\pm$ 0.000	0.241 $\pm$ 0.023	0.000 $\pm$ 0.000	<b>0.224 <math>\pm</math> 0.020</b>
		0.5	<b>0.184 <math>\pm</math> 0.004</b>	<b>0.247 <math>\pm</math> 0.024</b>	0.257 $\pm$ 0.008	0.279 $\pm$ 0.026
		0.2	<b>0.245 <math>\pm</math> 0.007</b>	<b>0.275 <math>\pm</math> 0.027</b>	0.482 $\pm$ 0.019	0.451 $\pm$ 0.042
		0.1	<b>0.357 <math>\pm</math> 0.016</b>	<b>0.362 <math>\pm</math> 0.029</b>	0.663 $\pm$ 0.029	0.634 $\pm$ 0.053
	192	1.	0.000 $\pm$ 0.000	0.254 $\pm$ 0.024	0.000 $\pm$ 0.000	<b>0.238 <math>\pm</math> 0.024</b>
		0.5	<b>0.184 <math>\pm</math> 0.005</b>	<b>0.240 <math>\pm</math> 0.026</b>	0.258 $\pm$ 0.006	0.280 $\pm$ 0.032
		0.2	<b>0.250 <math>\pm</math> 0.009</b>	<b>0.289 <math>\pm</math> 0.029</b>	0.481 $\pm$ 0.021	0.450 $\pm$ 0.054
		0.1	<b>0.372 <math>\pm</math> 0.017</b>	<b>0.388 <math>\pm</math> 0.030</b>	0.669 $\pm$ 0.030	0.650 $\pm$ 0.060
Traffic	96	1.	0.000 $\pm$ 0.000	0.222 $\pm$ 0.031	0.000 $\pm$ 0.000	<b>0.203 <math>\pm</math> 0.037</b>
		0.5	<b>0.219 <math>\pm</math> 0.017</b>	<b>0.224 <math>\pm</math> 0.033</b>	0.276 $\pm$ 0.012	0.255 $\pm$ 0.041
		0.2	<b>0.278 <math>\pm</math> 0.017</b>	<b>0.252 <math>\pm</math> 0.029</b>	0.532 $\pm$ 0.017	0.483 $\pm$ 0.040
		0.1	<b>0.418 <math>\pm</math> 0.019</b>	<b>0.382 <math>\pm</math> 0.014</b>	0.738 $\pm$ 0.023	0.721 $\pm$ 0.073
	192	1.	0.000 $\pm$ 0.000	0.215 $\pm$ 0.026	0.000 $\pm$ 0.000	<b>0.199 <math>\pm</math> 0.030</b>
		0.5	<b>0.211 <math>\pm</math> 0.014</b>	<b>0.216 <math>\pm</math> 0.028</b>	0.276 $\pm$ 0.011	0.245 $\pm$ 0.029
		0.2	<b>0.271 <math>\pm</math> 0.017</b>	<b>0.242 <math>\pm</math> 0.026</b>	0.532 $\pm$ 0.020	0.480 $\pm$ 0.050
		0.1	<b>0.397 <math>\pm</math> 0.025</b>	<b>0.360 <math>\pm</math> 0.022</b>	0.734 $\pm$ 0.022	0.787 $\pm$ 0.172